RSC Advances

ROYAL SOCIETY OF CHEMISTRY

www.rsc.org/advances

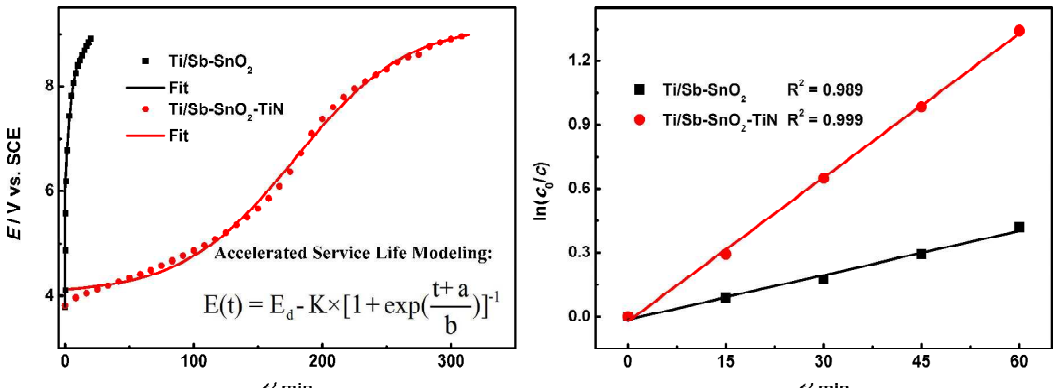

The Sb-doped SnO_2 electrode is modified by TiN nanoparticles and has higher stability and significantly enhanced electrochemical decolorization activity.

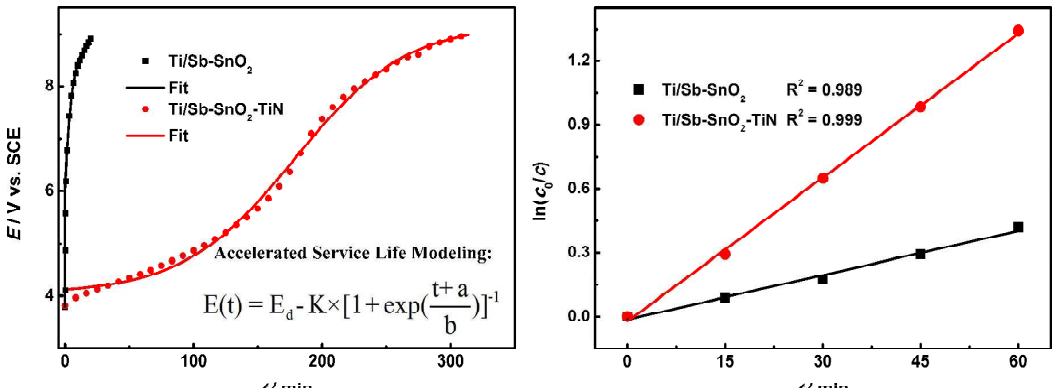

The Sb-doped SnO_2 electrode is modified by TiN nanoparticles and has higher stability and significantly enhanced electrochemical decolorization activity.

Enhanced Electrocatalytic Activity of Nano-TiN Composited Ti/Sb-SnO_2 Electrode Fabricated by Pulse Electrodeposition for Methylene Blue Decolorization

Tigang Duan, Ye Chen*, Qing Wen*, Ying Duan

Key Laboratory of Superlight Materials and Surface Technology of Ministry of Education, College of Material Science and Chemical Engineering, Harbin Engineering University, Harbin, 15001, Heilongjiang, China

*Corresponding author.

Tel.: +86-13059004260.

Fax: +86-451-82569792.

Email-address: chenye@hrbeu.edu.cn (Y Chen), wenqing@hrbeu.edu.cn (Q Wen).

Abstract: Ti/Sb-SnO_2 electrode modified with titanium nitride (TiN) nanoparticles was prepared by the pulse electro-codeposition method. X-ray diffraction and scanning electron microscopy show that compared with Ti/Sb-SnO_2, Ti/Sb-SnO_2-TiN electrode has a small unit cell volume of tetragonal SnO_2 and a refined, compact particle film. X-ray photoelectron spectroscopy analysis shows that introducing titanium nitride nanoparticles facilitates the formation of Sb^{5+}. And the adsorbed hydroxyl oxygen species content of Ti/Sb-SnO_2-TiN (43.07 %) is higher than that of Ti/Sb-SnO_2 (21.85 %), indicating that Ti/Sb-SnO_2-TiN electrode has more active sites for electrochemical oxidation of organic pollutants. In 0.25 M Na_2SO_4 solution, the charge transfer resistance of Ti/Sb-SnO_2-TiN (150 ohm) is much smaller than that of

Ti/Sb-SnO_2 (1334 ohm). With a constant current density of 100 mA cm^{-2}, the accelerated service lifetime of Ti/Sb-SnO_2-TiN is improved significantly, which is 15.7 times as long as that of Ti/Sb-SnO_2. Ti/Sb-SnO_2-TiN electrode is demonstrated to have a prominent ability for oxidative decolorization of methylene blue. The results also confirm that Ti/Sb-SnO_2-TiN electrode has higher decolorization efficiency and kinetic rate constant, which are 1.54 and 3.24 times as efficient as those of Ti/Sb-SnO_2, respectively.

Keywords: Titanium nitride; Sb-doped SnO_2; Voltammetric characterization; Accelerated life model.

1. Introduction

Electrochemical oxidation is an effective approach for treating organic wastewater, on account of its prominent oxidation performance, ease of operation and environmental compatibility.[1-3] For the application of electrochemical oxidation technology, appropriate electrodes with high electrochemical activity and long service life are essential.[4] There are different kinds of electrodes for electrochemical decomposition of organic pollutants, such as Pt, BDD, RuO_2, IrO_2, PbO_2, and MnO_2 electrodes. As one of semiconductor electrodes with a long history, Sb-doped SnO_2 electrode is early reported by Comninellis et al.[5] and is well known for its low cost, high oxygen evolution potential and electro-generation of hydroxyl radicals.[6] Higher oxygen evolution potential can restrain the subsidiary reaction of oxygen evolution,

and hydroxyl radicals can effectively suppress the electrode fouling and restore electrode activity.[7] Consequently, Sb-doped SnO_2 electrode is one of the most promising electrodes for electrochemical oxidation of organic pollutants.

Although Sb-doped SnO_2 electrode presents a superior electrocatalytic performance, it has a low stability for the irreversible deactivation, which is probably caused by substrate passivation and active substance consumption.[8,9] To overcome this disadvantage, some efforts for modifying electrodes have been taken considerably, including introduction of rare earths (Ce, Nd, Gd, Eu, Dy, Y, etc.) [10-13], doping with noble metals (Pt, Ru, Ir, etc.) [14-16], addition of other metals (Fe, Co, Ni, Bi, etc.) [17-20], and modification with interlayer[21]. Yang et al.[19] has studied the effects of rare earth (Ce), noble metals (Ru and Pd) and iron group metals (Fe, Co and Ni) on the performance of Sb-doped SnO_2 electrodes. And the results suggest that, in spite of the superior catalytic performance of nickel-modified electrode, the doping of rare earth Ce do not achieve a significant improvement for electrode activity, and that the introduction of Pd and Ru leads to a decrease of oxygen evolution potential which is unfavorable. Regarding the interlayer method, Wu et al.[22] have prepared Ti/TiN/Sb-SnO_2 electrodes with plasma sprayed TiN interlayer, but the conditions of interlayer fabrication is complicated. Considering about the factors mentioned above, there are some restrictions for these modification methods, and it is significant to explore some new ideas.

Recently, doping nanomaterials into active coatings has become a new focus for the modification of electrocatalytic electrodes. Hu and his co-workers[23,24] have

studied the impacts of carbon nanotubes and chromium carbides on Sb-doped SnO_2 electrodes, and it is satisfactory that the stability and activity of electrodes can both be improved. Zhang et al.[25] have prepared Sb-doped SnO_2 electrode modified with carbon nanotubes and have investigated the performance of electrochemical dye wastewater oxidation, and the results demonstrate a prominent enhancement for the stability and electrocatalytic activity.

Herein, titanium nitride nanoparticles are introduced to modify the electrocatalyitc electrodes. As one kind of metal nitrides, titanium nitride possesses some characteristics such as extreme hardness, high fire resistance, good electric conductivity, chemical stability, catalytic activity and relatively low costs.[26] Therefore, it is a desirable electrode material and can be good candidates for various applications including heterogeneous catalysis[27,28], hydrogen evolution electrocatalysis[29], water splitting photocatalysis[30], fuel cells[31,32], electrochemical capacitors[33], and solar cells[34]. However, the application of titanium nitride in the environmental field especially electrochemical wastewater treatment has not been reported widely. Nakayama et al.[35] have reported the application of titanium nitride for electrochemical inactivation of marine bacteria. And Su et al.[36] have reported the application of titanium nitride for electro-reduction debromination. The modification of electrocatalytic electrodes with titanium nitrides has not been reported frequently, either. On account of the electrochemical applications of titanium nitride, it is expected to apply to improving the stability and to promoting the performance for electrocatalytic electrodes through compositing titanium nitrides.

In this work, Ti/Sb-SnO_2-TiN electrode was fabricated by the pulse electro-codeposition method. Some characterizations, containing X-ray diffraction (XRD), scanning electron microscope (SEM), energy dispersive X-ray spectrometer (EDS) and X-ray photoelectron spectroscopy (XPS), were performed to test the crystal structure, morphology, surface composition and chemical states of oxygen element for Ti/Sb-SnO_2-TiN electrode. And the electrochemical experiments, including cyclic voltammetry (CV), electrochemical impedance spectroscopy (EIS) and chronopotentiommetry, were conducted to analyze the electrochemical activity and stability. The electrochemical oxidation decolorization of methylene blue was investigated to confirm the enhanced electrocatalytic performance of Ti/Sb-SnO_2-TiN electrode. Finally, an S-shaped curve equation was employed to evaluate the accelerated lifetime of electrode.

2. Experimental

2.1. Chemicals

All reagents were analytical grade and used without further purification. Titanium nitride nanoparticles (size 20 nm) were purchased from Aladdin Chemicals (Shanghai, China). Graphite rods (spectrum grade, diameter 8 mm) were from Sinopharm chemical reagent Co. Ltd (Shanghai, China).

2.2. Preparation of Ti/Sb-SnO_2-TiN composite electrodes

Ti sheets (0.5 mm thickness, 99.6 % purity) went through mechanically polishing, degreasing in a 10 % NaOH solution at 85 °C for 1 h, and etching in a 10 % oxalic acid solution at 85 °C for 2 h. Then pretreated Ti sheets were preserved in a 3 % oxalic acid solution.

0.024 g titanium nitride nanoparticles (20-50 nm) were mixed into the 100 mL electrodeposition solution consisting of 0.1 M $SnCl_4 \cdot 5H_2O$, 0.1 M citric acid and 0.011 M $SbCl_3$, and the mixed solution was ultrasonically dispersed for 5 min to obtain a homogeneous suspension with 0.24 g L^{-1} titanium nitride. Then ethylenediamine tetramethylenephosphonic acid was added dropwise to the electrolyte to obtain a 1 mM concentration. A graphite rod was employed as the anode, and Ti sheet as the cathode. Cathodic pulse electro-codeposition was performed for 0.5 h in the pulse conditions of 10 Hz frequency and 50 % duty percentage with an average current density of 5 mA cm^{-2}. To avoid the effect of temperature instability, the electrodeposition bath was kept at 23 °C. Deposited Ti sheets were washed by distilled water, then dried at 100 °C, and finally annealed in a muffle furnace at 500 °C for 1 h to obtain Ti/Sb-SnO_2-TiN electrodes. Scheme 1 shows the preparation of Ti/Sb-SnO_2-TiN electrode, and it is expected to obtain rough surface and improved electrode stability. The procedure to prepare Ti/Sb-SnO_2 electrode was the same as mentioned above, except adding titanium nitride nanoparticles.

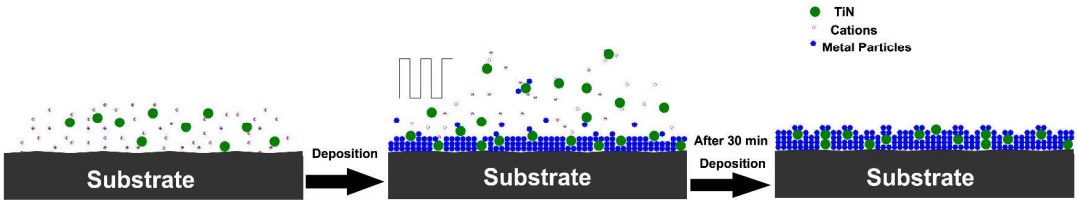

Scheme 1 Schematic illustration for the preparation of Ti/Sb-SnO_2-TiN electrode.

2.3. Characterization of electrodes

The morphologies of Ti/Sb-SnO_2-TiN composite electrodes were scanned and the elemental compositions were examined by scanning electron microscope (SEM; INSPECT S50, MAKE FEI, America) equipped with an energy dispersive X-ray spectrometer (EDS). X-ray diffraction (XRD; Rigaku D/Max2500, Japan) was performed with a Cu Kα radiation at 40 kV and 150 mA to obtain the crystalline patterns of tin oxide. X-ray photoelectron spectroscopy (XPS) measurements were performed on a Thermo ESCALAB 250 Electron Spectrometer (UK; Al Kα radiation, hν =1486.6 eV). The binding energy of C1s level from adventitious carbon at 284.6 eV was used as internal reference to calibrate the spectra.

2.4. Electrochemical experiments

Electrochemical experiments were performed in a conventional three-electrode cell recorded by a CHI760C electrochemical workstation (CH Instruments, China). The Ti/Sb-SnO_2-TiN composite electrode served as the working electrode with a test

area of 1 × 1 cm^2. A platinum sheet (2 × 2 cm^2) and saturated calomel electrode (SCE) were used as a counter and reference electrode, respectively. The electrolyte was 0.25 M Na_2SO_4 solution. Electrochemical impedance spectroscopy (EIS) measurements were conducted in a range of 10^5 Hz - 0.1 Hz and at a potential of 2.0 V (vs. SCE) with an amplitude signal of 5 mV, and the results ware fitted using the ZView software. Cyclic voltammetry (CV) was performed between 0.6 and 0.8 V with different sweep rates. Before each measurement, the system was stabilized at open circuit voltage for 5 - 10 min.

The accelerated service life tests were conducted using chronopotentiommetry with an anodic current density of 100 $mA \cdot cm^{-2}$ in the three-electrode system. The electrolyte was 0.25 M Na_2SO_4 solution. The anode potential was recorded as a function of time, and it indicated that the electrode was deactivated when the potential increased 5 V from its initial value.[37]

2.5. Dye decolorization tests

The electrochemical decolorization experiments for dyes (methylene blue-MB, methyl orange-MO, and orange II-OII) were performed in 50 mL 50 mg L^{-1} dye solution with the supporting electrolyte of 0.25 M Na_2SO_4 solution. The electrolysis was performed in the galvanostatic condition of 20 mA cm^{-2} with a working electrode area of 1 × 2 cm^2. The electrochemical decolorization process of dyes was monitored by the UV-Vis absorbance spectroscopy, and dye solution concentrations were

measured by the absorbance intensity at the characteristic wavelength of 664 nm (MB), 463nm (MO) and 484 nm (OII).

3. Results and discussion

3.1. Characterization of Ti/Sb-SnO_2 electrodes

The XRD patterns of Ti/Sb-SnO_2 and Ti/Sb-SnO_2-TiN electrodes are shown in Fig. 1. The diffraction peak positions for both samples coincide roughly with those of tetragonal rutile SnO_2 (PDF#41-1445) with the diffraction peaks appearing at (110), (101), (200), (211), (220), (310), (112), and (301). And several peak positions for both samples are related to the orthorhombic SnO_2 (PDF#29-1484). Regarding of orthorhombic SnO_2 phase, its formation is owed to a high stress inside the particle layer during oxidation.[38] Nevertheless, the additional peaks corresponding to antimony oxide are not found; this may be connected with either the low content of antimony element or the doping of antimony ions into the stannic oxide phase. No peaks for titanium oxides are observed, showing that the pulse electrodeposition process can produce a good coverage of the Ti matrix.

In Fig. 1(b), a significant increase arises up from the peak intensities of orthorhombic SnO_2. The weight ratio of orthorhombic to tetragonal SnO_2 can be estimated from the intensity ratio of the strongest orthorhombic peak to the intensity of the strongest tetragonal peak.[39] Thereby the content of orthorhombic SnO_2 for Ti/Sb-SnO_2-TiN is higher than that for Ti/Sb-SnO_2; this can be ascribed to a higher

stress caused by titanium nitrides. In addition, compared with that of Ti/Sb-SnO_2 electrode, the half peak widths at (110), (101) and (211) peaks for tetragonal SnO_2 of Ti/Sb-SnO_2-TiN electrode increase. As known by Scherrer's formula, the half peak width is inversely proportional to crystalline grain size, thus Ti/Sb-SnO_2-TiN electrode has a smaller crystal grain size. This result confirms that applying nanoparticles can refine the crystal grains, and thereby increase the specific surface area and active sites.

The lattice parameters (a=b and c) for Ti/Sb-SnO_2 and Ti/Sb-SnO_2-TiN electrodes were calculated by Bragg's formula based on the main diffraction peaks of tetragonal SnO_2 phase:

$$d_{hkl} = \frac{1}{\sqrt{((h^2 + k^2)/a^2) + (l^2/c^2)}} \quad (1)$$

where d_{hkl} is the crystal face space, h, k and l are crystal face index, and a and c are the unit-cell parameters.

The lattice parameters for Ti/Sb-SnO_2 electrode are $a = b = 4.730$ Å and $c = 3.187$ Å, and those for Ti/Sb-SnO_2-TiN electrode are $a = b = 4.730$ Å and $c = 3.178$ Å. The unit cell volume (V) was calculated by the formula $V = a^2 \times c$, and the results for both electrodes are 71.30 and 71.10 $Å^3$, respectively. This result shows that the lattice parameters and for both electrodes are smaller than those of the standard SnO_2 (cassiterite, $a = b = 4.738$ Å, $c = 3.187$ Å and $V = 71.54$ $Å^3$), which can be ascribed to the SnO_2 lattice distortion. Due to the fact that the radius of Sb^{5+} ion is smaller than that of Sn^{4+} ion, doping antimony ions into the stannic oxide crystalline lattices leads to the contraction of SnO_2 lattice parameters. Furthermore, with adding titanium

nitride nanoparticles, the unit cell volume of SnO_2 decreases from 71.30 $Å^3$ to 71.10 $Å^3$, suggesting more lattice distortions.

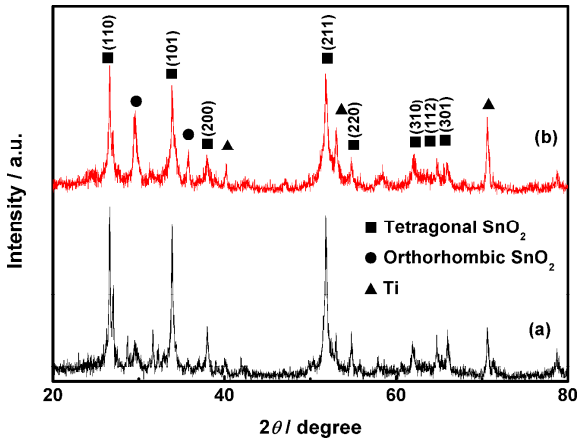

Fig. 1 XRD patterns of (a) Ti/Sb-SnO_2 electrode and (b) Ti/Sb-SnO_2-TiN electrode.

Fig. 2(a) and (b) show the SEM images of Ti/Sb-SnO_2 electrode and Ti/Sb-SnO_2-TiN electrodes. With increasing titanium nitride nanoparticles, particles of Ti/Sb-SnO_2-TiN electrode appear to be much smaller and more compact. Smaller particles have larger specific surface area and are expected to provide with more active sites for electrocatalytic oxidation. And a compact grains layer can cover Ti substrate and suppress the substrate oxidation so as to improve the electrode stability. Hence, Ti/Sb-SnO_2-TiN electrode can be expected to possess better electrochemical performance and stability. To observe the distribution of titanium nitrides in the deposited layer and to avoid Ti substrate disturbance, the EDS measurement of deposited layer on a copper foil was conducted (shown in Fig. 2(c) and (d)). The EDS result in Fig. 2(c) suggests the presence of O, Sn, Sb, Ti and N. The peaks of O, Sn and Sb elements are clearly observed, but Ti and N peaks can be insignificantly

observed. The atom percentages of O, Sn, Sb, Ti and N elements are 61.34 %, 30.99 %, 5.74 %, 1.08 % and 0.85 %, respectively. The lower content of N element than that of Ti element can be due to the thermal oxidation of titanium nitrides in air. X-ray dot-mapping is used for analyzing the distribution of layer elements, and Fig. 2(d) shows the Ti element distribution on the deposited layer. Titanium nitride nanoparticles are successfully doped in and relatively uniformly distributed on the deposited layer.

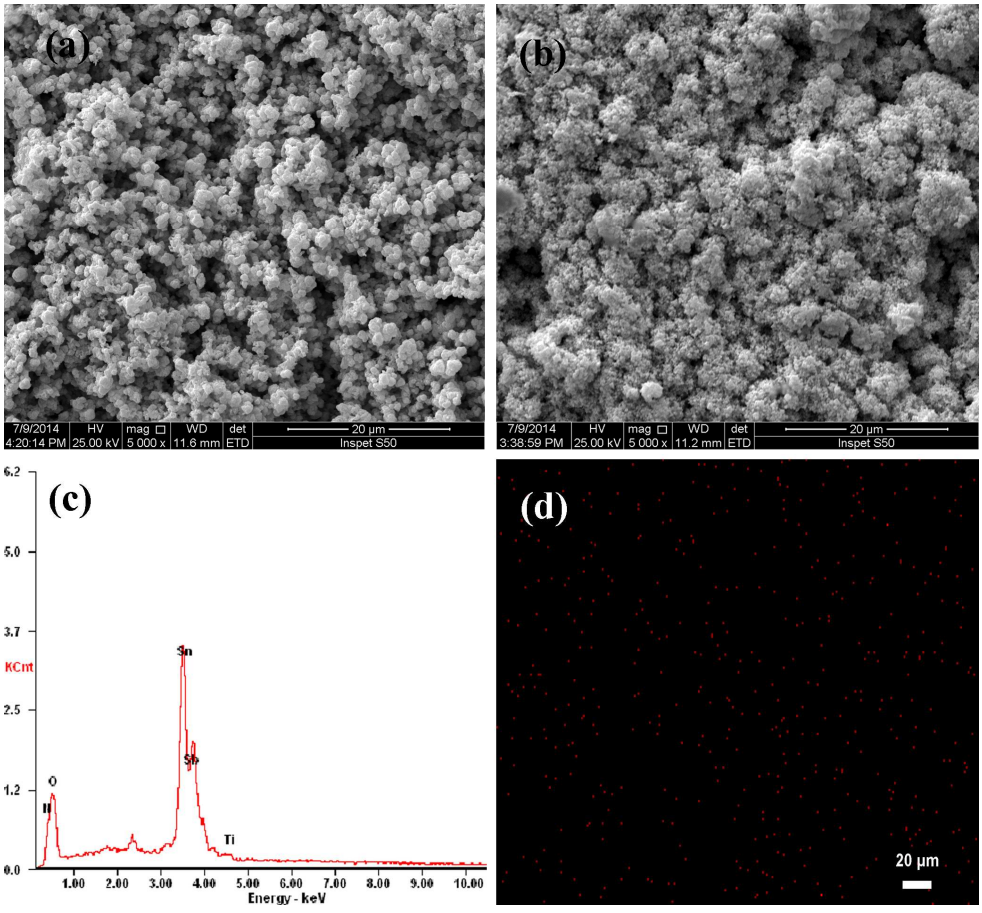

Fig. 2 SEM images of (a) Ti/Sb-SnO_2 electrode and (b) Ti/Sb-SnO_2-TiN electrode; (c) EDS result of the composite deposited layer and (d) X-ray dot-mapping of Ti element distribution on a copper substrate.

XPS is a surface analysis technique which can provide a good understanding of changes on the electrode surface, and thus XPS measurements of Ti/Sb-SnO_2 and Ti/Sb-SnO_2-TiN electrodes were conducted to analyze the chemical states of elements on the electrode surface. Survey spectra were recorded initially followed by narrow scan XPS spectra of Ti, Sn, Sb and O elements. Fig. 3 shows the element core-level spectra of the Ti/Sb-SnO_2 and Ti/Sb-SnO_2-TiN electrodes. They were fitted with the XPS Peak Processing software using Lorentzian-Gaussian peak shapes, and the fitted values were given in Tables 1 and 2.

The Ti 2p peaks of Ti/Sb-SnO_2-TiN electrode are shown in Fig. 3(a), where the high-resolution Ti 2p spectra shows four Ti 2p peaks arising at 456.91, 458.67, 461.06 and 465.27 eV, respectively. According to Avasarala and Haldar[40-41], the binding energies of Ti $2p_{3/2}$ and Ti $2p_{1/2}$ of electrode are assigned to titanium nitride, with 456.91 and 461.06 eV as their respective peak positions. Some titanium nitride nanoparticles undergoes a thermodynamically oxidation reaction when exposed to air[42]:

$$2TiN + 2O_2 \rightarrow 2TiO_2 + N_2 \uparrow \qquad (2)$$

Most of the substituted nitrogen is released in the interstitial positions of surface oxide layers as molecular nitrogen. Due to strongly thermal oxidation in air, the component of titanium oxide formed and the corresponding peaks are located at 458.67 and 465.27 eV, respectively. The inset of Fig. 3(a) shows the N 1s peak of Ti/Sb-SnO2-TiN electrode, demonstrating the existence of titanium nitrides. However,

possibly due to too low content of titanium nitride, the titanium nitride phase is not observed in the XRD (shown in Fig. 1).

Considering the effect of doping titanium nitride nanoparticles, further investigations were carried out. A comparison of the Sn 3d spectra of Ti/Sb-SnO_2 and Ti/Sb-SnO_2-TiN electrodes was shown in Fig. 3(b). The spectra reveal the spin-orbit of Sn $3d_{5/2}$ ground state in binding energy region of 486.7-486.8 eV while the Sn $3d_{3/2}$ excited state is observed in binding energy region of around 495.1-495.3 eV (Table 1), which is ascribed to Sn^{4+} in SnO_2.[43] The gap between the Sn $3d_{5/2}$ and Sn $3d_{3/2}$ levels is about 8.4 eV, which closely corresponds to the O in SnO_2 and Sn in SnO_2, respectively.[44] It is observed that the binding energy of Sn 3d for Ti/Sb-SnO_2-TiN electrode is slightly higher than that for Ti/Sb-SnO_2 electrode, indicating a lower electron density around the Sn^{4+} in Ti/Sb-SnO_2-TiN as a result of more lattice O^{2-} existing in the crystal lattice.[12]

The XPS spectra of Sb $3d_{5/2}$ and O 1s are overlapped, thus they were fitted and split into three peaks, and the fitted values are given in Table 1 and Table 2. And to investigate the doping effect on the chemical state of Sb, the Sb $3d_{3/2}$ peak was split into two peaks assigned to Sb^{3+} and Sb^{5+}, respectively, which are displayed in the insets of Figs. 3(c) and (d). Observed from Table 1, the atom ratio of Sn and Sb for both electrodes is around 4.2, showing that introducing nanoparticles dose not influence evidently the content of Sn and Sb in the active layer; EDS result shows that the atom ratio of Sn and Sb for electrode before annealing is 4.9 which is higher than that after annealing. This phenomenon can be ascribed to the segregation of antimony

element on the electrode surface[45]. However, the atom ratio of Sb^{5+} and Sb^{3+} is boosted from 2.2 to 6.5 with doping titanium nitrides. This result can give an explanation for the unit volume decreasing of Ti/Sb-SnO_2-TiN electrode.

It is generally considered that the O 1s peak is observed in binding energy region of 529-535 eV. Two O 1s peaks, which are a lower binding energy peak at about 530.3-530.4 eV and a higher binding energy peak at about 531.6-531.8 eV, can be observed. Babar et al.[44] attributed the lower energy binding peak to the lattice oxygen species (O_L), and Srinivas et al.[46] assigned the higher energy binding peak to adsorbed hydroxyl oxygen species (O_{ad}). The relative content of two kinds of oxygen species was estimated preliminarily by the peak-area ratio method. The molar ratio of adsorbed hydroxyl oxygen and lattice oxygen for the Ti/Sb-SnO_2-TiN electrode is 75.67 %, which is higher than that for Ti/Sb-SnO_2 electrode. And with doping titanium nitride nanoparticles, the atom ratio of O_{ad} and O_L increases from 21.85 % to 43.07 %. O_{ad} plays a prominent role in the oxidation process and influences the catalytic activity of electrodes.[47] Therefore, the increased O_{ad} content implies that the electrochemical activity of Ti/Sb-SnO_2-TiN electrode will be considerably influenced by titanium nitrides.

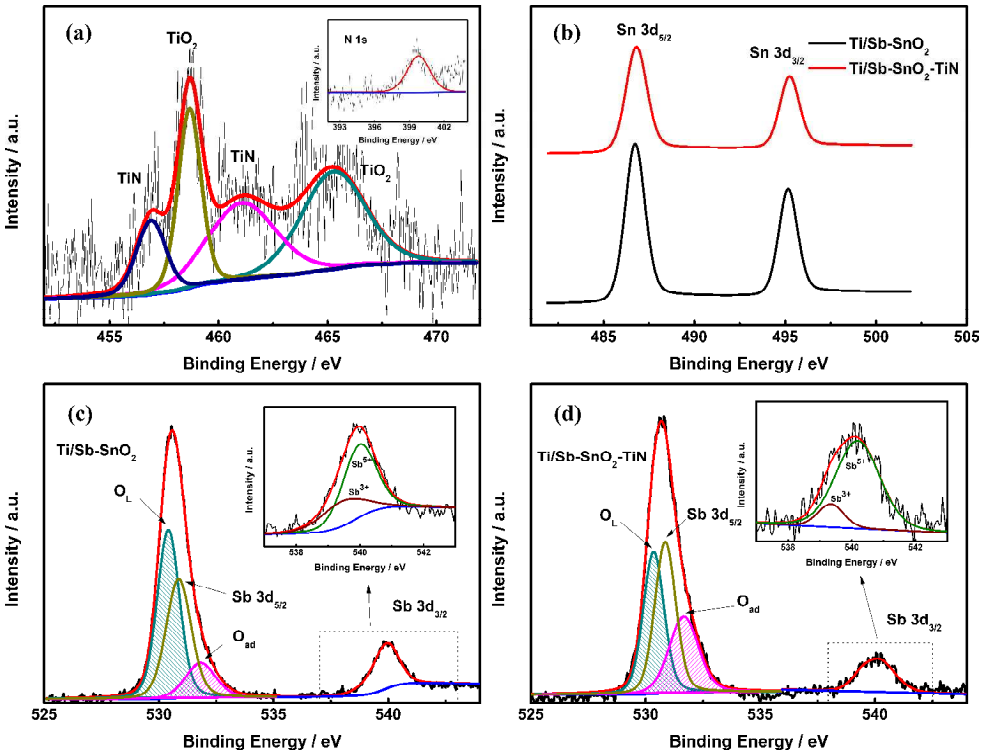

Fig. 3 (a) Ti 2p core-level XPS for Ti/Sb-SnO_2-TiN electrode, (b) Sn 3d core-level XPS for Ti/Sb-SnO_2 and Ti/Sb-SnO_2-TiN electrodes, (c) and (d) O 1s and Sb 3d core-level XPS for Ti/Sb-SnO_2 and Ti/Sb-SnO_2-TiN electrodes. The inset is the N 1s core-level XPS for Ti/Sb-SnO_2-TiN electrode.

Table 1 XPS data of chemical states of tin and antimony elements on the electrode surface.

Sample	Binding Energy / eV				Atom ratio of	Atom ratio of
	Sn $3d_{5/2}$	Sn $3d_{3/2}$	Sb $3d_{5/2}$	Sb $3d_{3/2}$	Sn: Sb	Sb^{5+}: Sb^{3+}
Ti/Sb-SnO_2	486.73	495.16	530.67	540.05	4.21	2.21
Ti/Sb-SnO_2-TiN	486.80	495.24	530.86	540.13	4.13	6.51

Table 2 XPS data of chemical states of oxygen element on the electrode surface.

Sample	Binding energy / eV	Atomic ratio of O_{ad}: O_L / %	O_{ad} content / %

	O1s (O_L)	O1s (O_{ad})		($Content = \frac{O_{ad}}{O_{ad}+O_L} \times 100\%$)
Ti/Sb-SnO_2	530.41	531.82	27.96	21.85
Ti/Sb-SnO_2-TiN	530.35	531.67	75.67	43.07

3.2 Effects of the amount of titanium nitride nanoparticles

EIS is a good approach to study the interfacial phenomenon, and herein is employed to investigate the electrochemical performance of various titanium nitride modified tin dioxide based electrodes. EIS experiments were performed at room temperature with a potential of 2.0 V (vs. SCE). Fig. 4 shows the experimental and fitted EIS spectra for various Ti/Sb-SnO_2-TiN electrodes. In order to interpret the EIS spectra, the equivalent circuit was used to fit and to model the EIS behavior shown in the inset of Fig. 4(a). The Nyquist plots for all electrodes are similar in form, and are characterized by one resistance in higher frequency region, one capacitive-resistive semicircle in high frequency region and the other depressed capacitive-resistive semicircle in low frequency region. The resistance in higher frequency region corresponding to resistance (R_1) in the model represents the solution resistance. The semicircle in high frequency region, which corresponds to the capacitance (C_2) and resistance (R_2) in the model, is supposed to represents the electrochemical behavior of the growth of a resistive hydrated layer at the oxide/solution interface[48]. It is considered to be associated with the properties of layers[49] with no well understanding.

The depressed semicircle in low frequency, which behaves as the constant phase

element (CPE_3) and charge transfer resistance (R_3) in the equivalent circuit, represents the electrochemical discharge process, and its behavior demonstrates the electrochemical performance of electrodes. A high capacitance (corresponding to CPE_3) in the depressed semicircle can arise from a rough surface and reflect a high specific area[50], and a low charge transfer resistance (corresponding to R_3) can reflect a good electrochemical activity. Simulation parameters of EIS data were listed in Table 3. As can be seen from Table 3, the CPE_3 and R_3 values for different Ti/Sb-SnO_2-TiN electrodes vary with the amount of titanium nitrides. When the concentration of titanium nitrides is 0.24 g L^{-1}, the electrochemical activity of electrode is optimal. The CPE_3 value for Ti/Sb-SnO_2-TiN electrode is 2.04×10^{-3} F, 5.1 times of that for Ti/Sb-SnO_2 electrode, implying a significant enhancement of specific area. And the R_3 value of Ti/Sb-SnO_2-TiN (0.24) electrode is only 150 ohm while that for Ti/Sb-SnO_2 electrode is 1334 ohm, showing a prominent improvement of electrocatalytic performance for electrodes. These results may be ascribed to the decreased unit cell volume of SnO_2 caused by the introduction of titanium nitrides, and thus reveal the contribution of titanium nitrides to the improved electrode activity.

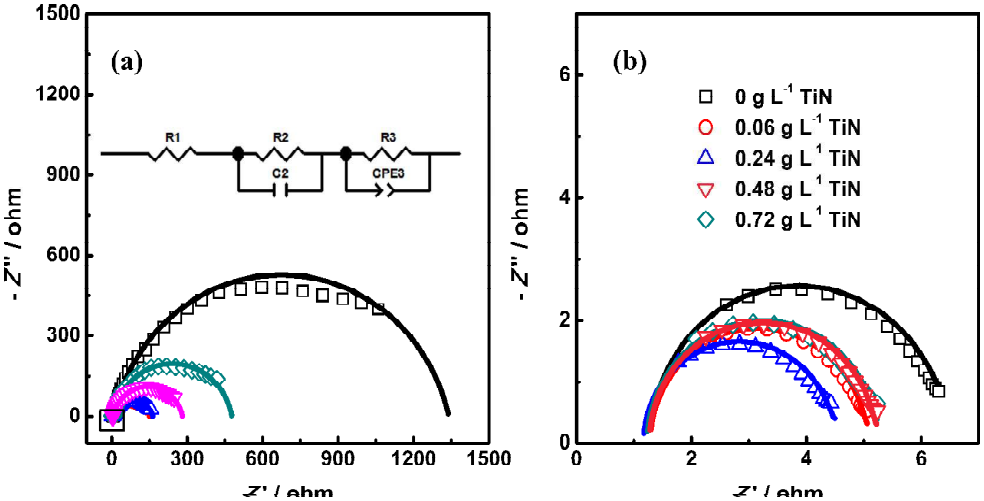

Fig. 4 (a) Electrochemical impedance spectra (Nyquist plots) of Ti/Sb-SnO_2-TiN electrodes with different nano-TiN amounts in a 0.25 M Na_2SO_4 solution, and (b) corresponding local amplificatory plots. The inset is fitted equivalent circuit model.

Table 3 EIS analysis results of Ti/Sb-SnO_2 electrodes with different titanium nitride compositing amounts.

TiN concentration / g L^{-1}	R_1/ohm	R_2/ohm	C_2/F	R_3/ohm	CPE_3/F	n
0	1.28	5.05	5.58×10^{-7}	1334	4.00×10^{-4}	0.85
0.06	1.28	3.73	7.19×10^{-7}	159	1.94×10^{-3}	0.82
0.24	1.17	3.28	7.07×10^{-7}	150	2.04×10^{-3}	0.83
0.48	1.27	3.92	7.38×10^{-7}	276	1.61×10^{-3}	0.86
0.72	1.23	3.98	8.04×10^{-7}	472	1.00×10^{-3}	0.88

To investigate the effects of amounts of titanium nitrides on the electrocatalytic activity of electrodes, electrochemical decolorization of methylene blue were performed on different Ti/Sb-SnO_2-TiN electrodes for 1 h electrolysis time. And the

electrolysis was performed in 50 mL 50 mg L^{-1} methylene blue and 0.25 M Na_2SO_4 mixed solution with the galvanostatic condition of 20 mA cm^{-2}, and the electrode area is 1 × 2 cm^2. Fig. 5 shows the variations of one-hour methylene blue decolorization efficiency with TiN concentration. The decolorization percentage of Ti/Sb-SnO_2 electrode without titanium nitrides is only 34.3 %. However, it significantly increases with doping titanium nitride nanoparticles. With increasing the amount of titanium nitride nanoparticles, the methylene blue decolorization efficiency presents a parabola change. And the 0.24 g L^{-1} group presents an optimal decolorization efficiency of 61.2 %, revealing the most significant electrocatalytic activity. The decolorization process for methylene blue will be further discussed in the following analysis.

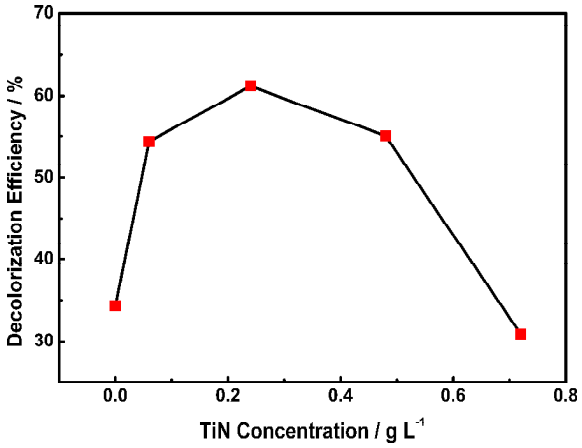

Fig. 5 Effects of TiN concentration on the decolorization efficiency of methylene blue.

3.3. Voltammetric characterization

In order to explain the effect of doping titanium nitride nanoparticles on the electrocatalytic activity of electrodes, the relative roughness factor (R_f) and

voltammetric charge of both electrodes were determined from CV.

The relative roughness factor reflecting the real surface area of electrode is defined as real surface area per apparent geometric area of electrode, and calculated through comparing determined capacitance with the capacitance of a smooth oxide surface (60 $\mu F \cdot cm^{-2}$).[51] Figs. 6(a) and (b) show cyclic voltammgrams between 0.6 and 0.8 V at different sweep rates for both electrodes, and insets are plots of current densities at 0.7 V against sweep rates. The current densities were measured in the points of 0.7 V from the CV with 0.6 - 0.8 V potential range for different sweep rates. The linear relationship between current density and sweep rate confirms the nonfaradaic character of the current in this potential region .[52] The capacitances were obtained from the plot slopes in Figs. 6(a) and (b), and they were compared with the value of 60 $\mu F \cdot cm^{-2}$ to estimate the roughness factor. Compared with that of Ti/Sb-SnO_2, the relative roughness factor of Ti/Sb-SnO_2-TiN is boosted (43.50 versus 14.27, Table 4). Thus, the introduction of titanium nitride nanoparitcles can improve remarkably the roughness of electrode surface and is favorable to the electrocatalytic activity.

The voltammetric charge (q^*) is closely related to the real specific surface area and the amounts of electroactive sites, which greatly determines the electrocatalytic performance of electrode[53]. The total voltammetric charge q_T^*, which is related to the total electrochemically active surface area of the oxide coating, can be obtained through plotting the reciprocal of q^* against the square root of the potential scan rate by using the following equation[54]:

$$1/q^* = 1/q_T^* + kv^{1/2} \qquad (3)$$

The outer voltammetric charge q_O^*, which is the charge related to the most accessible electroactive surface area, is obtained according to the following equation:

$$q^* = q_O^* + k'v^{-1/2} \qquad (4)$$

In addition, the inner voltammetric charge q_I^*, is calculated from the total and outer charge by subtraction.

Figs. 6(c) and (d) show these plots for Ti/Sb-SnO_2 and Ti/Sb-SnO_2-TiN electrodes and good linear fittings can be observed. As seen from Fig. 6(c), Ti/Sb-SnO_2-TiN electrode appears larger q_{total}^* value, showing that introducing titanium nitrides significantly improves the electrochemically active surface area. Fig. 6(d) shows the relationship between q^* and $v^{-1/2}$ and that the value of outer voltammetric charge is obviously increased. This result shows that the TiN-modified electrode can provide with the more active sites for the electrocatalytic process. The values of voltammetric charges for both electrodes were listed in Table 4. Seen from Table 4, the values of q_{total}^* and q_{outer}^* for Ti/Sb-SnO_2-TiN are 4.50 and 3.60 times as large as those for Ti/Sb-SnO_2, respectively. These results indicate that the electrode modified with titanium nitrides has higher effective electrochemical surface area.

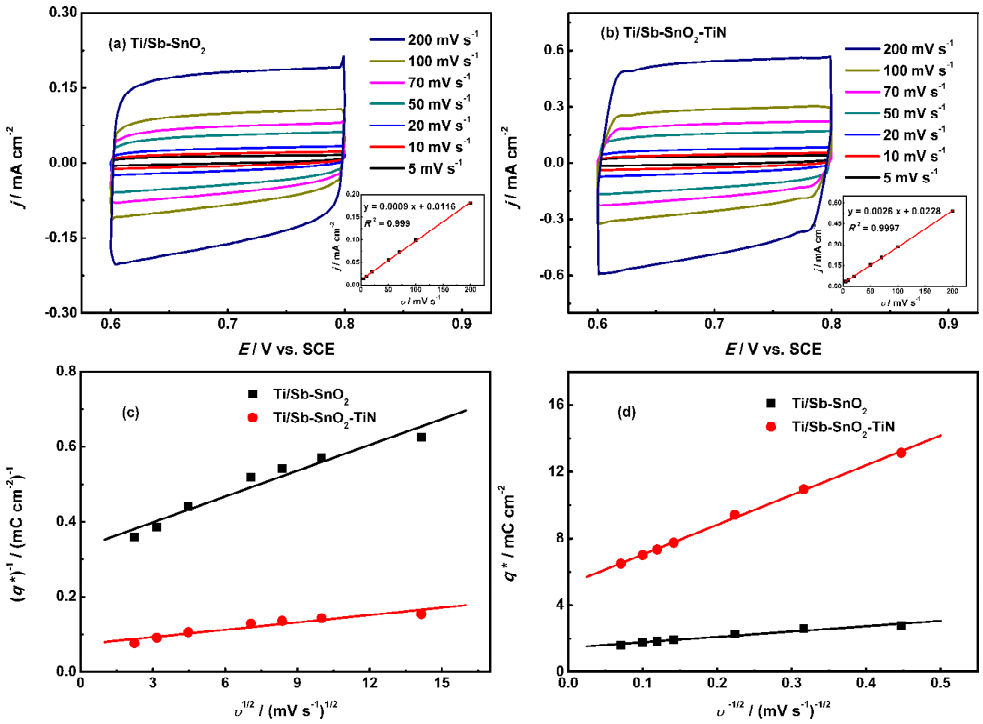

Fig. 6 Cyclic voltammograms for (a) Ti/Sb-SnO_2 and (b) Ti/Sb-SnO_2-TiN electrodes with sweep rates from 5 to 200 mV s^{-1} in 0.25 M Na_2SO_4 solution. Insets are linear regression of j versus v measured at E = 0.7 V. (c) Reciprocal voltammetric charge ($1/q^*$) versus the square root of the voltammetric scan rate ($v^{1/2}$) for Ti/Sb-SnO_2 and Ti/Sb-SnO_2-TiN electrodes. (d) Voltammetric charge (q^*) versus the reciprocal square root of the voltammetric scan rate ($v^{-1/2}$) for Ti/Sb-SnO_2 and Ti/Sb-SnO_2-TiN electrodes. (c) and (d) data was obtained from the cyclic voltammograms between 0.5 and 1.5 V at various scan rates in 0.25 M Na_2SO_4 solution.

Table 4 The roughness factors and voltammetric charges of Ti/Sb-SnO_2 and Ti/Sb-SnO_2-TiN electrodes.

Sample	R_f	q_{total}^* / mC cm^{-2}	q_{outer}^* / mC cm^{-2}
Ti/Sb-SnO_2	14.27	3.03	1.46
Ti/Sb-SnO_2-TiN	43.50	13.65	5.25

3.4. Electrochemical decolorization performance

To examine the electrochemical decolorization performance of Ti/Sb-SnO_2 and Ti/Sb-SnO_2-TiN electrodes, the adsorption and decolorization processes of methylene blue were performed on both electrodes. To enhance the decolirization ability, it is very helpful to increase the adsorption capacity of dye contaminant on the electrode surface. Fig. 7(a) shows the variations of adsorption efficiency with time. The adsorptions increase with time, and the adsorption balance is achieved after approximately 1 h. After 2 h adsorption, the efficiencies are 3.4 % and 8.9 %, respectively, demonstrating a higher adsorption capacity of Ti/Sb-SnO_2-TiN electrode. This can be due to the result that Ti/Sb-SnO_2-TiN electrode possesses a higher roughness and more electroactive sites. The higher concentration of contaminants maintaining around the electrode, to some extent, can inhibit the decolorization decay and improve the efficiency.

Fig. 7(b) shows the decolorization efficiency (η), calculated according to Equation (5), with the variation of time:

$$\eta(\%) = \frac{A_0 - A}{A_0} \times 100 \qquad (5)$$

where A_0 and A are the absorbance at the initial time and t (min), respectively. Methylene blue solution concentrations were measured by the absorbance intensity at the characteristic wavelength of 664 nm.

Observed from Fig. 7(b), methylene blue decolorization efficiencies increase with electrolysis time. And methylene blue solution is decolorized rapidly on

Ti/Sb-SnO_2-TiN electrode but decolorized slowly on Ti/Sb-SnO_2 electrode, showing that the methylene blue decolorization on Ti/Sb-SnO_2-TiN is much more efficient than that on Ti/Sb-SnO_2. The difference of methylene blue decolorization increases with the electrolysis proceeding. During 60 min electrolysis, the methylene blue decolorization efficiencies of Ti/Sb-SnO_2-TiN and Ti/Sb-SnO_2 electrodes rise and reach 73.9 % and 34.3 %, respectively. The electrochemical decolorization efficiency for Ti/Sb-SnO_2-TiN within 90 min is obviously higher than that for Ti/Sb-SnO_2 within 120 min. After 120 min, the methylene blue decolorization efficiencies are 100 % and 65.1 %, respectively. This result reveals that the activity of Ti/Sb-SnO_2-TiN electrode is higher than that of Ti/Sb-SnO_2 electrode.

The inset of Fig. 7(b) shows the semi-log relationship of methylene blue concentration with electrolysis time. Dye decolorization process is considered to follow the pseudo-first order kinetics model[55-56]:

$$dc / dt = -kc \qquad (6)$$

Where c is the concentration of methylene blue at given time and k is the kinetic rate constant. The kinetic rate constants for methylene blue decolorization were obtained from the slope of the inset curve in Fig. 7(b). They are 6.96×10^{-3} min^{-1} for Ti/Sb-SnO_2 and 22.5×10^{-3} min^{-1} for Ti/Sb-SnO_2-TiN. This shows that methylene blue can be decolorized far more rapidly on Ti/Sb-SnO_2-TiN electrode and that the decolorization rate constant for Ti/Sb-SnO_2-TiN is 3.24 times as efficient as that for Ti/Sb-SnO_2.

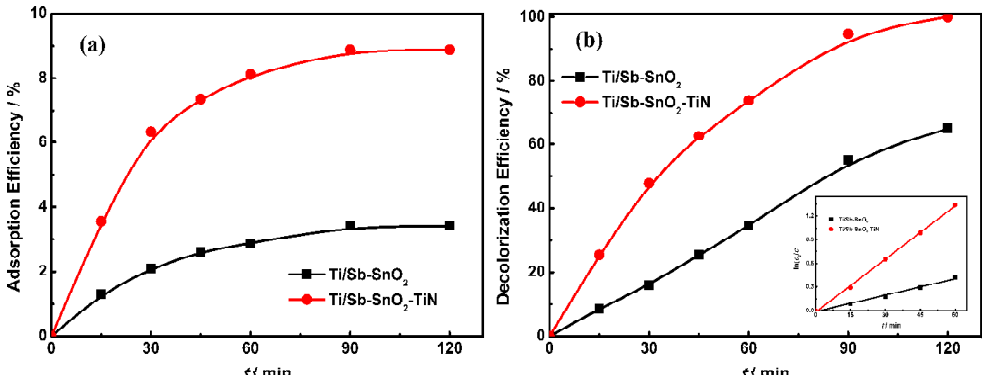

Fig. 7 Variations of (a) adsorption efficiency, and (b) decolorization efficiency with time. The inset is the pseudo-first order of methylene blue decolorization on Ti/Sb-SnO_2 and Ti/Sb-SnO_2-TiN electrodes. The adsorption and electrolysis were performed in 50 mL 50 mg L^{-1} methylene blue and 0.25 M Na_2SO_4 mixed solution in magnetic stirring with the electrode area is 1 × 2 cm^2. And the electrolysis was under the galvanostatic condition of 20 mA cm^{-2}.

To further investigate the electrocatalyitc decolorization ability of Ti/Sb-SnO_2-TiN electrode, the electrochemical decolorization processes of methylene blue with different concentrations, methyl orange and orange II were performed. Fig. 8(a) shows the decolorization performance of Ti/Sb-SnO_2-TiN against different concentrations of methylene blue. With increasing the dye concentration, the decolorization efficiencies and kinetics rate constants decrease. As the dye concentration is increased from 50 to 150 mg L^{-1}, the decolorization efficiency still reaches up to 93.4 %, and the kinetics rate constant is 18.54×10^{-3} min^{-1}. And as the concentration is further increased to 300 mg L^{-1}, the dye decolorization amount increases from the original 50 mg L^{-1} to 201.3 mg L^{-1} although the decolorization efficiency is 67.1 %. This result indicates that the TiN-modified electrode has good

decolorization ability for relatively high concentration of methylene blue dye.

Fig. 8(b) shows the decolorization ability of Ti/Sb-SnO_2-TiN electrode against different dyes with the same concentrations. After 60 min electrolysis, the decolorization efficiencies of methylene blue, methyl orange, and orange II on Ti/Sb-SnO_2-TiN electrode are 73.9 %, 89.9 % and 77.7 %, respectively. After 120 min, the decolrization efficiencies are 100 %, 94.7 % and 94.2 %, respectively. And the pseudo-first order kinetics rate constants are 22.5, 39.5 and 24.5 min^{-1}, respectively. Observed from the pseudo-first order kinetic rate constant comparison of different electrodes in Table 5, it is demonstrated that the TiN-modified electrode has a high decolorization performance for different dyes. This result shows that Ti/Sb-SnO_2-TiN electrode has a wide use for the decolorization of different dyes.

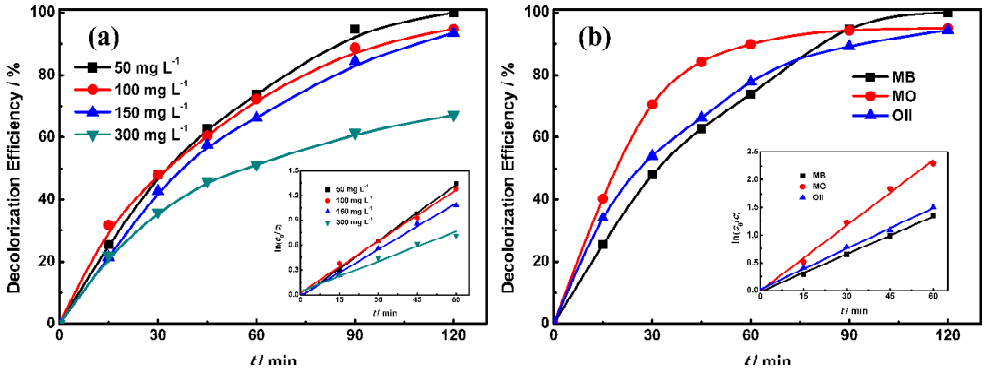

Fig. 8 Decolorization efficiencies of (a) methylene blue with different concentrations, and (b) different dyes. The insets are the pseudo-first order of dye decolorization on Ti/Sb-SnO_2-TiN electrode.

Table 5 Pseudo-first order kinetic rate constant comparison of different electrodes.

References	Electrode	Electrolysis Condition	k / 10^{-3} min^{-1}
[57]	Pt	100 mg L^{-1} methyl violet, 0.05 M Na_2SO_4,	1.13;

[58]	BDD	pH=3, 33.3 mA cm^{-2}	31.1
	MMO	50 mg L^{-1} methyl orange, 0.1 M Na_2SO_4,	2.48
	BDD	pH=3, 50 mA cm^{-2}	15.4
[59]	Ti/PbO_2-ZrO_2	30 mg L^{-1} MB, 0.25 M Na_2SO_4, 50 mA cm^{-2}	24.3
[25]	Ti/SnO_2-Sb;	1 g L^{-1} C.I. Acid Red 73, 0.1 M Na_2SO_4,	8.3;
	Ti/SnO_2-Sb-CNT	50 mA cm^{-2}	16.0
[60]	Ti/Sb-SnO_2;	50 mg L^{-1} MB, 0.25 M Na_2SO_4,	6.11;
	Ti/Sb-SnO_2-NGNS	20 mA cm^{-2}	36.6
This work	Ti/Sb-SnO_2;	50 mg L^{-1} MB, 0.25 M Na_2SO_4,	6.96;
	Ti/Sb-SnO_2-TiN	20 mA cm^{-2}	22.5;
This work	Ti/Sb-SnO_2-TiN	50 mg L^{-1} MO, 0.25 M Na_2SO_4, 20 mA cm^{-2}	39.5
This work	Ti/Sb-SnO_2-TiN	50 mg L^{-1} OII, 0.25 M Na_2SO_4, 20 mA cm^{-2}	24.5

Electrochemical oxidation decolorization of methylene blue was monitored with UV-Vis absorbance spectroscopy. The UV-Vis spectra of methylene blue were reported in Fig. 9, and changes in the spectra demonstrate the decolorization of methylene blue quantitatively. The UV-Vis absorbance peaks of initial methylene blue solution appear at wavelengths of 664 nm, 293 nm and 246 nm. Among those absorbance peaks, the peak at 664 nm can be ascribed to dimenthylamino group as the

chromophore, and the two peaks in the ultraviolet region are attributed to the benzene rings in the methylene blue molecule.[61] With increasing electrolysis time, all characteristic peaks of methylene blue decrease. Due to the N-demethylation and deamination of methylene blue, the absorbance peak at 664 nm for Ti/Sb-SnO_2-TiN electrode decreases rapidly till disappearing, suggesting a complete electrochemical decolorization after 2 h electrolysis. The absorbance peaks at 293 nm and 246 nm decrease in the consequence of benzene ring cracking. During the electrochemical decolorization process, no new peaks appear, implying a complete oxidative decomposition of methylene blue. Therefore, N-demethylation, deamination and electrochemically oxidative decomposition occur when the electrochemical decolorization proceeds.

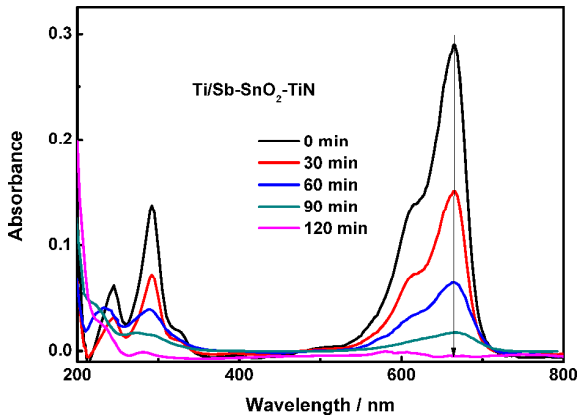

Fig. 9 Changes in the UV-Vis absorbance spectrum of methylene blue after different time intervals on Ti/Sb-SnO_2-TiN electrode.

The stability is always an important factor, thus we nade the reusability test on electrocatalytic oxidation of methylene blue; namely, reuse the electrodes after first catalytic run and redo the methylene blue decolorization test in a fresh solution.

Meanwhile, the XRD measurement of the electrodes after electro-decolorization was also performed to study the crystalline structure. Fig. 10(a) shows the changes of decolorization efficiencies with electrode use times. After 10 times decolorization, the decolorization efficiency is still up to 99.1 %, demonstrating a high stability for the electrode activity. Observed from XRD of Ti/Sb-SnO_2-TiN electrodes with 1, 4, 7 and 10 use times shown in Fig. 10(b), all the electrodes have good degree of crystallinity. The lattice parameters of Ti/Sb-SnO_2-TiN (1) electrode are $a = b = 4.738$ Å and $c = 3.230$ Å, which are higher than those of the fresh electrode ($a = b = 4.730$ Å and $c = 3.178$ Å). This may indicate that Ti/Sb-SnO_2-TiN electrode needs stabilization treatment before use. And with increasing the decolorization times, the lattice parameters of electrodes are not increased and keep constant. This result shows that Ti-modified electrodes have good stability.

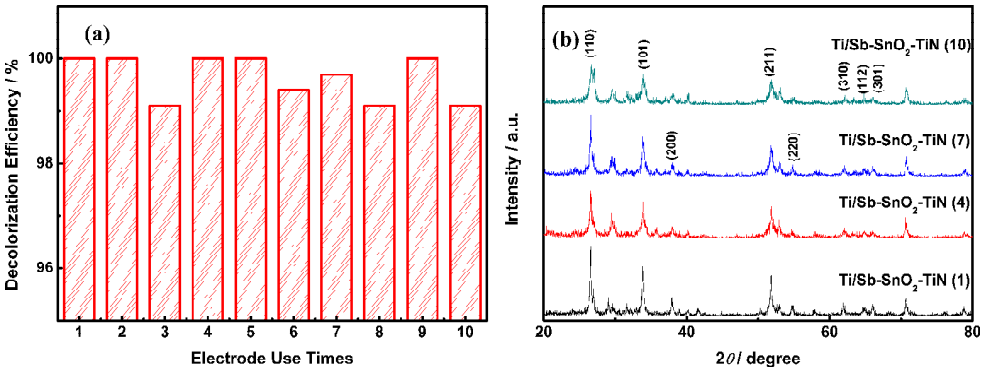

Fig. 10 (a) Changes of decolorization efficiencies with electrode use times on the same Ti/Sb-SnO_2-TiN electrode; (b) XRD patterns of Ti/Sb-SnO_2-TiN electrodes with different use times.

3.5. Kinetics model for estimating electrode deactivation

The electrochemical stability is an important factor related with the electrode quality. The stabilities of Ti/Sb-SnO_2 and Ti/Sb-SnO_2-TiN electrodes were investigated through accelerated service life tests with an anodic current density of 100 $mA \cdot cm^{-2}$, as shown in Fig. 11. At a high current density, severe oxygen evolution reaction occurs on the electrode surface, and can lead to Ti substrate passivation and active substance consumption in the consequence of an irreversible electrode deactivation.[9] The accelerated service lifetime for Ti/Sb-SnO_2 electrode is only 0.33 h. Compositing titanium nitrides into electrode prolongs the accelerated life to 5.22 h, which is 15.7 times as long as that for Ti/Sb-SnO_2 electrode. Ti/Sb-SnO_2-TiN electrode presents an improved accelerated life and can be ascribed to the compact composite layer due to the impact of titanium nitrides.

To describe the electrode deactivation process during the accelerated service life experiment, as one kind of S-shaped curve equations, logistic curve equation is used to fit the accelerated service life curve. Ti/Sb-SnO_2 electrode demonstrates a sharp increase in potential and gets deactivated within twenty minutes, indicating its low electrochemical stabilization:

$$E(t) = 8.87 - 11791 \times [1 + \exp(\frac{t + 44.1}{5.29})]^{-1}, \text{ with } R^2 = 0.980 \qquad (7)$$

The situation for Ti/Sb-SnO_2-TiN electrode is very different, and the accelerated service life curve changes in a sigmoid type increase. At first, the potential increases gradually for the initial period, then increases rapidly for the next period. Finally, the change of accelerated service life curve is towards stabilization in the high potential,

indicating the electrode deactivation. The following equation is obtained:

$$E(t) = 9.21 - 5.18 \times [1 + \exp(\frac{t - 179}{43.8})]^{-1}, \text{ with } R^2 = 0.997 \qquad (8)$$

The fitting degrees (R^2) of accelerated service life curves are more than 0.98, thus the logistic curve equation can well describe the electrode deactivation for the accelerated service life:

$$E(t) = E_d - K \times [1 + \exp(\frac{t + a}{b})]^{-1} \qquad (9)$$

Seen from Equation (6) and (7), E_d is the final potential when the electrode is deactivated, the values of K, a and b determine the accelerated service life of electrode.

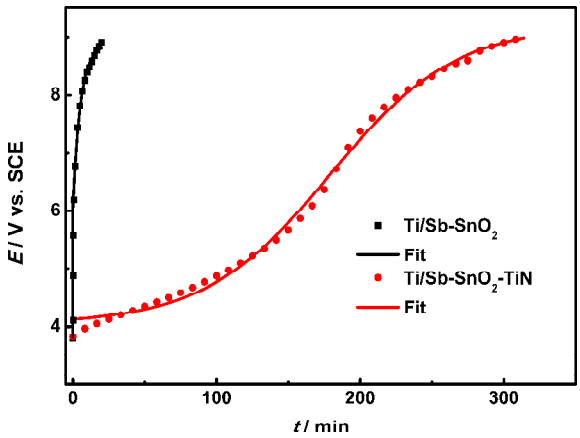

Fig. 11 Accelerated service life tests on (■) Ti/Sb-SnO_2 and (●) Ti/Sb-SnO_2-TiN electrodes in a 0.25 M Na_2SO_4 solution with an anodic current density of 100 mA cm^{-2}.

4. Conclusions

An effective Ti/Sb-SnO_2-TiN electrode was successfully fabricated by the pulse electro-codeposition method. Compared with Ti/Sb-SnO_2, Ti/Sb-SnO_2-TiN electrode has smaller lattice size and compact layer which can provide with more active sites.

XPS analysis shows that introducing titanium nitrides facilitates the formation of Sb^{5+} and increases the content of adsorbed hydroxyl oxygen. Voltammetric characterization shows that Ti/Sb-SnO_2-TiN electrode possesses larger relative roughness factor and voltammetric charge, indicating a higher electrocatalytic activity. The kinetic analysis shows that the electrochemical oxidation decolorization process of methylene blue coincides with the pseudo-first order kinetics and that the rate constant on Ti/Sb-SnO_2-TiN electrode is 22.52×10^{-3} min^{-1}, 3.24 times as efficient as that on Ti/Sb-SnO_2. Therefore, the TiN-modified Ti/Sb-SnO_2 electrode presents a high electrocatalytic activity and can have a good prospect for the electrochemical wastewater treatment.

Acknowledgment

The project was supported by National Natural Science Foundation of China (No. 51179033 and No. 21476053), the Doctoral Program of the Ministry of Education (No. 20132304110027), the Fundamental Research Funds for the Central Universities, and Special Fund Research Program for Talents of Science Technology Innovation in Harbin (No. 2009RFXXG204).

References

[1] G. Chen, Electrochemical technologies in wastewater treatment, *Sep. Purif.*

Technol., 2004, **38**, 11-41.

[2] C.A. Martínez-Huitle, S. Ferro, Electrochemical oxidation of organic pollutants for the wastewater treatment: direct and indirect processes, *Chem. Soc. Rev.*, 2006, **35**, 1324-1340.

[3] A. Anglada, A. Urtiaga, I. Ortiz, Contributions of electrochemical oxidation to waste-water treatment: fundamentals and review of applications, *J. Chem. Technol. Biotechnol.*, 2009, **84**, 1747-1755.

[4] G. Zhao, X. Cui, M. Liu, Peiqiang Li, Y. Zhang, T. Cao, H. Li, Y. Lei, L. Liu, D. Li, Electrochemical degradation of refractory pollutant using a novel microstructured TiO_2 nanotubes/Sb-doped SnO_2 electrode, *Environ. Sci. Technol.*, 2009, **43**, 1480-1486.

[5] C. Comninellis, C. Pulgarin, Electrochemical oxidation of phenol for wastewater treatment using SnO_2 anodes, *J. Appl. Electrochem.*, 1993, **23**, 108-112.

[6] T. Wu, G. Zhao, Y. Lei, P. Li, Distinctive Tin dioxide anode fabricated by pulse electrodeposition: high oxygen evolution potential and efficient electrochemical degradation of fluorobenzene, *J. Phys. Chem. C*, 2011, **115**, 3888-3898.

[7] K.R. Saravanan, S. Sathyamoorthi, D. Velayutham, V. Suryanarayanan, Voltammetric investigations on the relative deactivation of boron-doped diamond, glassy carbon and platinum electrodes during the anodic oxidation of substituted phenols in room temperature ionic liquids, *Electrochim. Acta*, 2012, **69**, 71-78.

[8] B. Correa-Lozano, C. Comninellis, A.D. Battisti, Service life of Ti/SnO_2-Sb_2O_5 anodes, *J. Appl. Electrochem.*, 1997, **27**, 970-974.

[9] X. Chen, G. Chen, P.L. Yue, Stable Ti/IrO_x-Sb_2O_5-SnO_2 anode for O_2 evolution with low Ir content, *J. Phys. Chem. B*, 2001, **105**, 4623-4628.

[10] Y. Feng, Y. Cui, B. Logan, Z. Liu, Performance of Gd-doped Ti-based Sb-SnO_2 anodes for electrochemical destruction of phenol, *Chemosphere*, 2008, **70**, 1629-1636.

[11] Y. Feng, Y.H. Cui, J. Liu, B.E. Logan, Factors affecting the electro-catalytic characteristics of Eu doped SnO_2/Sb electrode, *J. Hazard. Mater.*, 2010, **178**, 29-34.

[12] Y.H. Cui, Y.J. Feng, Z.Q. Liu, Influence of rare earths doping on the structure and electro-catalytic performance of Ti/Sb-SnO_2 electrodes, *Electrochim. Acta*, 2009, **54**, 4903-4909.

[13] L. Xu, Z. Guo, L. Du, Anodic oxidation of azo dye C.I. Acid Red 73 by the yttrium-doped Ti/SnO_2-Sb electrodes, *Front. Chem. Sci. Eng.*, 2013, **7**, 338-346.

[14] B. Adams, M. Tian, A. Chen, Design and electrochemical study of SnO_2-based mixed oxide electrodes, *Electrochim. Acta*, 2009, **54**, 1491-1498.

[15] Y. Liu, H. Liu, J. Ma, J. Li, Preparation and electrochemical properties of Ce-Ru-SnO_2 ternary oxide anode and electrochemical oxidation of nitrophenols, *J. Hazard. Mater.*, 2012, **213-214**, 222-229.

[16] G. Chen, X. Chen, P.L. Yue, Electrochemical behavior of novel Ti/IrO_x-Sb_2O_5-SnO_2 anodes, *J. Phys. Chem. B*, 2002, **106**, 4364-4369.

[17] D. He, S. Mho, Electrocatalytic reactions of phenolic compounds at ferric ion co-doped SnO_2:Sb^{5+} electrodes, *J. Electroanal. Chem.*, 2004, **568**, 19-27.

[18] P.A. Christensen, K. Zakaria, H. Christensen, T. Yonar, The effect of Ni and Sb oxide precursors, and of Ni composition, synthesis conditions and operating

parameters on the activity, selectivity and durability of Sb-doped SnO_2 anodes modified with Ni**,** *J. Electrochem. Soc.*, 2013, **160**, H405-H413.

[19] S.Y. Yang, Y.S. Choo, S. Kim, S.K. Lim, J. Lee, H. Park, Boosting the electrocatalytic activities of SnO_2 electrodes for remediation of aqueous pollutants by doping with various metals, *Appl. Catal. B-Environ.*, 2012, **111-112**, 317-325.

[20] Q. Zhuo, S. Deng, B. Yang, J. Huang, G. Yu, Efficient electrochemical oxidation of perfluorooctanoate using a Ti/SnO_2-Sb-Bi anode, *Environ. Sci. Technol.*, 2011, **45**, 2973-2979.

[21] D. Shao, W. Yan, X. Li, H. Yang, H. Xu, A highly stable Ti/TiH_x/Sb-SnO_2 anode: preparation, characterization and application, *Ind. Eng. Chem. Res.*, 2014, **53**, 3898-3907.

[22] X. Wu, J. Zhang, Y. Wang, A. Huang, Structure and properties of Ti/TiN/Sb-SnO_2 electrodes with plasma sprayed TiN interlayer, *Adv. Mater. Res.*, 2013, **602-604**, 1613-1616.

[23] F. Hu, X. Cui, W. Chen, Pulse Electro-codeposition of Ti/SnO_2-Sb_2O_4-CNT electrode for phenol oxidation, *Electrochem. Solid-State Lett.*, 2010, **13**, F20-F23.

[24] F. Hu, Z. Dong, X. Cui, W. Chen, Improved SnO_2-Sb_2O_4 based anode modified with Cr_3C_2 and CNT for phenol oxidation, *Electrochim. Acta*, 2011, **56**, 1576-1580.

[25] L. Zhang, L. Xu, J. He, J. Zhang, Preparation of Ti/SnO_2-Sb electrodes modified by carbon nanotube for anodic oxidation of dye wastewater and combination with nanofiltration, *Electrochim. Acta*, 2014, **117**, 192-201.

[26] J.G. Chen, Carbide and nitride overlayers on early transition metal surfaces:

preparation, characterization, and reactivities, *Chem. Rev.*, 1996, **96**, 1477-1498.

[27] J.S.J. Hargreaves, Heterogeneous catalysis with metal nitrides, *Coordin. Chem. Rev.*, 2013, **257**, 2015-2031.

[28] A.M. Alexander, J.S.J. Hargreaves, Alternative catalytic materials: carbides, nitrides, phosphides and amorphous boron alloys, *Chem. Soc. Rev.*, 2010, **39**, 4388-4401.

[29] W.F. Chen, J.T. Muckerman, E. Fujita, Recent developments in transition metal carbides and nitrides as hydrogen evolution electrocatalysts, *Chem. Commun.*, 2013, **49**, 8896.

[30] Y. Moriya, T. Takata, K. Domen, Recent progress in the development of (oxy) nitride photocatalysts for water splitting under visible-light irradiation, *Coordin. Chem. Rev.*, 2013, **257**, 1957-1969.

[31] D.J. Ham, J.S. Lee, Transition metal carbides and nitrides as electrode materials for low temperature fuel cells, *Energies*, 2009, **2**, 873-899.

[32] S. Dong, X. Chen, X. Zhang, G. Cui, Nanostructured transition metal nitrides for energy storage and fuel cells, *Coordin. Chem. Rev.*, 2013, **257**, 1946-1956.

[33] D. Choi, P.N. Kumta, Nanocrystalline TiN derived by a two-step halide approach for electrochemical capacitors, *J. Electrochem. Soc.*, 2006, **153**, A2298-A2303.

[34] Q.W. Jiang, G.R. Li, X.P. Gao, Highly ordered TiN nanotube arrays as counter electrodes for dye-sensitized solar cells, *Chem. Commun.*, 2009, **44**, 6720-6722.

[35] T. Nakayama, H. Wake , K. Ozawa, H. Kodama, N. Nakamura, T. Matsunaga, Use of a titanium nitride for electrochemical inactivation of marine bacteria, *Environ.*

Sci. Technol., 1998, **32**, 798-801.

[36] J. Su, N. Lu, J. Zhao, H. Yu, H. Huang, X. Dong, X. Quan, Nano-cubic structured titanium nitride particle films as cathodes for the effective electrocatalytic debromination of BDE-47, *J. Hazard. Mater.*, 2012, **231-232**, 105-113.

[37] Y. Chen, L. Hong, H. Xue, W. Han , L. Wang, X. Sun, J. Li, Preparation and characterization of TiO_2-NTs/SnO_2-Sb electrodes by electrodeposition, *J. Electroanal. Chem.*, 2010, **648**, 119-127.

[38] A.D. Garje, R.C. Aiyer, Effect of firing temperature on electrical and gas-sensing properties of nano-SnO_2-based thick-film resistors, *Int. J. Appl. Ceram. Tec.*, 2007, **4**, 446-452.

[39] S. Tian, Y. Gao, D. Zeng, C. Xie, Effect of zinc doping on microstructures and gas-sensing properties of SnO_2 nanocrystals, *J. Am. Ceram. Soc.*, 2012, **95**, 436-442.

[40] B. Avasarala, P. Haldar, Electrochemical oxidation behavior of titanium nitride based electrocatalysts under PEM fuel cell conditions, *Electrochim. Acta*, 2010, **55**, 9024-9034.

[41] B. Avasarala, P. Haldar, On the stability of TiN-based electrocatalysts for fuel cell Applications, *Int. J. Hydrogen Energ.*, 2011, **36**, 3965-3974.

[42] G. Hyett, M.A. Green, I.P. Parkin, The use of combinatorial chemical vapor deposition in the synthesis of $Ti_{3-\delta}O_4N$ with $0.06<\delta<0.25$: a titanium oxynitride phase isostructural to anosovite, *J. Am. Chem. Soc.*, 2007, **129**, 15541-15548.

[43] D. Kim, S. Kim, AFM observation of ITO thin films deposited on polycarbonate substrates by sputter type negative metal ion source, *Surf. Coat. Tech.*, 2003, **176**,

23-29.

[44] A.R. Babar, S.S. Shinde, A.V. Moholkar, C.H. Bhosale, J.H. Kim, K.Y. Rajpure, Sensing properties of sprayed antimony doped tin oxide thin films: solution molarity, *J. Alloy. Compd.*, 2011, **509**, 3108-3115.

[45] B. Slater, C.R.A. Catlow, D.H. Gay, D.E. Williams, V. Dusastre, Study of surface segregation of antimony on SnO_2 surfaces by computer simulation techniques, *J. Phys. Chem. B*, 1999,**103**, 10644-10650.

[46] K. Srinivas, M. Vithal, B. Sreedhar, M.M. Raja, P.V. Reddyhave, Structural, optical, and magnetic properties of nanocrystalline Co doped SnO_2 based diluted magnetic semiconductors, *J. Phys. Chem. C*, 2009, **113**, 3543-3552.

[47] D. Pavlov, The lead-acid battery lead dioxide active mass: a gel-crystal system with proton and electron conductivity, *J. Electrochem. Soc.*, 1992, **139**, 3075-3080.

[48] A. Chen, S. Nigro, Influence of a nanoscale gold thin layer on Ti/SnO_2-Sb_2O_5 electrodes, *J. Phys. Chem. B*, 2003, **107**, 13341-13348.

[49] A. Oury, A. Kirchev, Y. Bultel, Oxygen evolution on alpha-lead dioxide electrodes in methanesulfonic acid, *Electrochim. Acta*, 2012, **63**, 28-36.

[50] X. Yang, J. Kirsch, J. Fergus, A. Simonian, Modeling analysis of electrode fouling during electrolysis of phenolic compounds, *Electrochim. Acta*, 2013, **94**, 259-268.

[51] D. Santos, M.J. Pacheco, A. Gomes, A. Lopes, L. Ciríaco, Preparation of Ti/Pt/SnO_2-Sb_2O_4 electrodes for anodic oxidation of pharmaceutical drugs, *J. Appl. Electrochem.*, 2013, **43**, 407-416.

[52] F. Montilla, E. Morallón, A. De Battisti, S. Barison, S. Daolio, J.L. Vázquez, Preparation and characterization of antimony-doped tin dioxide electrodes. part 1. electrochemical characterization, *J. Phys. Chem. B*, 2004, **108**, 5036-5043.

[53] L.K. Xu, J.D. Scantlebury, Electrochemical surface characterization of IrO_2-Ta_2O_5 coated titanium electrodes in Na_2SO_4 solution, *J. Electrochem. Soc.*, 2003, **150**, B288-B293.

[54] S. Ardizzone, G. Fregonara, S. Trasatti, "Inner" and "outer" active surface of RuO_2 electrodes, *Electrochim. Acta*, 1990, **35**, 263-267.

[55] B. Haspulat, A. Gülce, H. Gülce, Efficient photocatalytic decolorization of some textile dyes using Fe ions doped polyaniline film on ITO coated glass substrate, *J. Hazard. Mater.*, 2013, **260**, 518-526.

[56] G. Zhao, J. Li, X. Ren, J. Hu, W. Hu, X. Wang, Highly active MnO_2 nanosheet synthesis from grapheme oxide templates and their application in efficient oxidative degradation of methylene blue, *RSC Adv.*, 2013, **3**, 12909-12914.

[57] M. Hamza, R. Abdelhedi, E. Brillas, I. Sirés, Comparative electrochemical degradation of the triphenylmethane dye Methyl Violet with boron-doped diamond and Pt anodes, *J. Electroanal. Chem.*, 2009, **627**, 41-50.

[58] M. Zhou, H. Särkkä, M. Sillanpää, A comparative experimental study on methyl orange degradation by electrochemical oxidation on BDD and MMO electrodes, *Sep. Purif. Technol.*, 2011, **78**, 290-297.

[59] Y. Yao, C. Zhao, M. Zhao, X. Wang, Electrocatalytic degradation of methylene blue on PbO_2-ZrO_2 nanocomposite electrodes prepared by pulse electrodeposition, *J.*

Hazard. Mater., 2013, **263**, 726-734.

[60] T. Duan, Q. Wen, Y. Chen, Y. Zhou, Y. Duan, Enhancing electrocatalytic performance of Sb-doped SnO_2 electrode by compositing nitrogen-doped graphene nanosheets, *J. Hazard. Mater.*, 2014, **280**, 304-314.

[61] X. Liang, Y. Zhong, S. Zhu, L. Ma, P. Yuan, J. Zhu, H. He, Z. Jiang, The contribution of vanadium and titanium on improving methylene blue decolorization through heterogeneous UV-Fenton reaction catalyzed by their co-doped magnetite, *J. Hazard. Mater.*, 2012, **199-200**, 247-254.